

Toward Macro-Modeling of Alkali-Silica Reaction-Affected Structures

by Anca C. Ferche, Daman K. Panesar, Shamim A. Sheikh, and Frank J. Vecchio

Although much attention has been directed toward modeling alkali-silica reaction (ASR) since its first deleterious effects on concrete structures were identified 75 years ago, there remain many unresolved issues. Among them, according to CSA A864-00, is that conventional methods of analysis become invalid for the assessment of ASR-affected structures due to the induced anisotropy with regards to the mechanical properties of concrete. To address this need, an alternative procedure for nonlinear analysis of ASR-affected reinforced concrete structures is presented, implemented within the framework of finite-element programs developed for the analysis of membrane and three-dimensional structures. Reinforced concrete is treated as an orthotropic material based on a smeared rotating crack model within the context of a total-load secant-stiffness macro-modeling approach. Verification is provided through analyses of reinforced concrete beams with behavior governed by either flexural or shear mechanisms.

Keywords: alkali-silica reaction; analysis; assessment; finite element; nonlinear analysis; reinforced concrete; structures.

INTRODUCTION

Chemical deterioration of concrete in the form of alkali-aggregate reaction (AAR) is a slowly-evolving and progressive process leading to expansion and cracking of concrete. AAR is a chemical reaction between alkali hydroxides (sodium and potassium) from portland cement or from an external source and certain reactive aggregates. Two main types of AAR are currently recognized based on the type of reactive minerals involved in the reaction: alkali-silica reaction (ASR) and alkali-carbonate reaction (ACR).

Problems due to ASR were first identified in California in the 1920s and 1930s when several structures developed cracks early in their service life, although the proper standards of the time had been applied during their construction. Studies conducted by Stanton^{1,2} showed that the expansion of concrete was caused by the chemical reaction between alkali from cement and siliceous aggregates. Stanton also identified the role of alkali content in the reaction, and the capacity of pozzolanic material to prevent the expansion.

Reported for the first time in Ontario in the 1950s,³ ACR is a chemical reaction between the alkali from the cement paste and certain carbonate rocks, particularly calcitic dolomite and dolimitic limestones. The reaction is usually accompanied by dedolomitization and expansion of the affected aggregate particles, leading to abnormal expansion and cracking of concrete in service. In 1982, another mechanism of chemical deterioration of concrete was reported: delayed ettringite formation (DEF), a form of sulfate attack common in concrete exposed to high temperatures during the curing process. The presence of products of both ASR and DEF has been identified during structure diagnosis.⁴ As such, several experimental studies have been carried out to investigate the

interaction of the two reactions,^{5,6} identifying similar deleterious effects on concrete.

The ASR mechanism, the far more widespread of the AAR reactions, is the focus of this work. One of the most extensively used methods for quantitatively assessing the deterioration caused by ASR is the Damage Rating Index (DRI). Studies⁷⁻⁹ have shown a good correlation between the DRI and the expansion levels measured. The DRI grading procedure has proven to be a reliable performance indicator and a solid starting basis for structural assessment in cases where coring is permitted. The subsequent step should consist of evaluating the mechanical properties of the concrete. Previous studies^{7,10} using nondestructive testing (NDT) techniques have shown that a relatively good correlation can be found for the modulus of elasticity of the concrete; however, the compressive and tensile strengths of ASR-affected concrete cannot be accurately determined using NDT. Another option for approximating the concrete's mechanical soundness, based on ISE¹¹ recommendations, involves use of expressions relating the estimated linear free expansion and the unaffected mechanical property values at 28 days. However, for anisotropic expansion levels and concrete subjected to different stress state conditions, ISE¹¹ does not provide comprehensive guidance.

A series of challenges arise when evaluating the behavior of structures affected by ASR, as follows:

1. The influence of restraint on the structural effects of ASR is not yet fully understood.
2. In the case of complex stress states, the anisotropy of the mechanical properties of concrete caused by the anisotropic ASR expansion is expected to be increased.
3. A comprehensive mathematical model to describe the anisotropy of the expansion as a result of casting direction and geometric configuration of the concrete element is not currently available.
4. The in-place material properties are usually difficult to obtain; destructive testing may not be an option, and nondestructive testing methods may face challenges due to high steel congestion, accessibility, presence of liners, or large thickness of the sections.

Several theoretical, semi-empirical, and numerical constitutive models have been developed to reproduce the ASR effect at a material or structural scale. Depending on the level at which the ASR is described, three types of models can be identified: micro-models, meso-models, and macro-models.

ACI Structural Journal, V. 114, No. 5, September-October 2017.

MS No. S-2016-117.R2, doi: 10.14359/51700778, received January 12, 2017, and reviewed under Institute publication policies. Copyright © 2017, American Concrete Institute. All rights reserved, including the making of copies unless permission is obtained from the copyright proprietors. Pertinent discussion including author's closure, if any, will be published ten months from this journal's date if the discussion is received within four months of the paper's print publication.

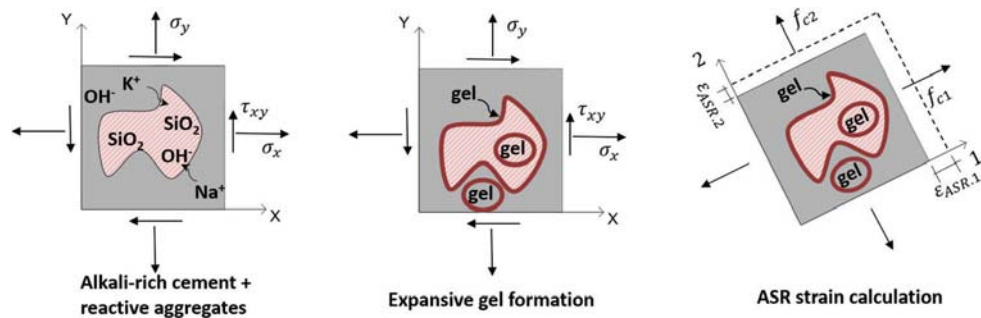


Fig. 1—ASR-induced strain calculation.

In micro-models, the emphasis lies in developing transport equations for the reactants and the diffusion processes to quantify the gel formation and its swelling; the aggregate and the cement paste are typically modeled separately.¹²⁻¹⁴ The meso-models are focused on dimensions between 10 and 100 mm (0.394 and 3.94 in.)—a scale that encompasses the aggregates, the interfacial transition zone, and the cement paste. At this level, the concrete is modeled as a heterogeneous material to better understand and capture the local mechanisms of deformation and their effect on the changes on the microstructure.¹⁵

The emphasis of macro-models lies with the global behavior of a structure affected by ASR, taking into consideration the deformations, the stresses, and the deleterious cracking. There are numerous models in the literature; most of them were formulated within the framework of a finite element method. Some models decouple the structural modeling from the reaction mechanism, other models couple them, and yet some others ignore reaction kinetics. The reaction kinetics is typically based on experimental studies while the behavior of concrete is simulated as either linear elastic or nonlinear. Some approaches previously presented in the literature adopt an elasto-plastic behavior for concrete¹⁶ or a visco-elasto-plastic damage model,¹⁷ while others are based on a smeared fixed crack model.^{18,19}

An alternative approach for structural assessment, based on a smeared rotating crack formulation within a macro-modeling framework, is proposed herein. The two-phase analysis consists of first evaluating the ASR strains based on long-term stress conditions, followed by the calculation of the specimen's behavior and capacity under a specific short-term loading scenario. The analytical procedure has been devised to account for the effects of lateral expansion, cyclic loading, tension stiffening, tension softening, compression softening, and bond-slip mechanisms among others.

RESEARCH SIGNIFICANCE

Structures identified as suffering from ASR require, in most cases, structural assessment. There is a need for improved analysis tools and ASR numerical models to decipher the observed behavior, predict long-term effects, assess potential damage or failure mechanisms, and facilitate rehabilitation works. This paper presents an analytical procedure suited for the nonlinear analysis of ASR-affected structures. The procedure is validated through simulations of behavior for reinforced concrete beams affected by ASR. Important

mechanisms that need to be captured in the analysis are identified, and future research recommendations are made.

FINITE ELEMENT IMPLEMENTATION

Two distinct (but not independent) mechanisms have to be considered to model the effects of ASR on reinforced concrete: the nature and magnitude of the chemically-induced expansion, and the resulting changes in the mechanical properties of the concrete. In both respects, models currently available in the literature were successfully implemented into two in-house nonlinear finite element programs developed at the University of Toronto for the analysis of reinforced concrete structures. The programs employ a smeared rotating crack model for concrete suitable for a macro-modeling approach; one is applicable to concrete membrane structures, while the other is appropriate for the analysis of three-dimensional (3-D) structures. The Modified Compression Field Theory (MCFT)²⁰ and the Disturbed Stress Field Model (DSFM)²¹ form the theoretical basis for both programs. The solution procedure uses an incremental total-load, iterative secant stiffness formulation with the constitutive, compatibility, and equilibrium relationships formulated in terms of average stresses and average strains.^{22,23}

ASR-induced strain calculation

ASR expansion is treated as an offset strain, evaluated in an iterative manner in the first load stage of the analysis (that is, representing average long-term in-place loading conditions) according to a procedure previously developed for elastic and plastic offset strains.²⁴ Six different models for the evaluation of ASR-induced expansion were implemented: uniform in all directions, Charlwood model,²⁵ Curtis model (personal communication, Aug. 19, 2014), Saouma and Perotti model,²⁶ Sellier model,²⁷ and Gautam model.⁷ Apart from the model that distributes ASR strains uniformly in all directions, the others calculate anisotropic expansion along the principal directions as a function of the stress state (Fig. 1). The level of expansion developed under stress-free conditions is a required parameter for the ASR analysis. It may be directly input by the user, or it may be evaluated using the Saouma and Perotti²⁶ or Sellier et al.²⁷ models, which include a kinetics component. Thus, provided that experimental data describing the reaction, specific to each model, are available from laboratory tests, the free expansion may be determined.

The total strains $[\epsilon]$ at a point in a reinforced concrete continuum represent the summation of: the net concrete

stress-induced strains $[\epsilon_c]$; the elastic concrete strain offsets $[\epsilon_c^o]$ due to mechanisms such as thermal expansion, prestrains, shrinkage, and lateral expansion; the plastic concrete strain offsets $[\epsilon_c^p]$ due to cyclic loading or damage effects; and the strains due to shear slip along the crack $[\epsilon^s]$. Consequently, the compatibility relationship for concrete in two dimension is

$$[\epsilon] = [\epsilon_c] + [\epsilon_c^o] + [\epsilon_c^p] + [\epsilon^s] \quad (1)$$

$$[\epsilon] = \begin{bmatrix} \epsilon_x \\ \epsilon_y \\ \gamma_{xy} \end{bmatrix}; [\epsilon_c] = \begin{bmatrix} \epsilon_{cx} \\ \epsilon_{cy} \\ \gamma_{cxy} \end{bmatrix}; [\epsilon_c^o] = \begin{bmatrix} \epsilon_{cx}^o \\ \epsilon_{cy}^o \\ \gamma_{cxy}^o \end{bmatrix}; [\epsilon_c^p] = \begin{bmatrix} \epsilon_{cx}^p \\ \epsilon_{cy}^p \\ \gamma_{cxy}^p \end{bmatrix}; [\epsilon^s] = \begin{bmatrix} \epsilon_x^s \\ \epsilon_y^s \\ \gamma_{xy}^s \end{bmatrix} \quad (2)$$

The relationship was modified to accommodate the anisotropic expansion due to ASR, which is handled in the same manner as the thermal or shrinkage strains. ASR-induced strains are evaluated for a stress condition representing the average long-term loading condition during which ASR expansion occurred; these strains and their orientations are then held constant and carried through subsequent analyses as elastic strain offsets in the prestrain vector $[\epsilon_c^o]$. They are determined with respect to the principal axes according to one of the ASR constitutive models implemented; thus ϵ_{c1}^o , ϵ_{c2}^o , ϵ_{c3}^o are found. If angle θ defines the orientation of the principal axes, the following relationships are used for transforming the strains to the x,y reference system

$$\epsilon_{cx,ASR}^o = \epsilon_{c1,ASR}^o \frac{(1 + \cos 2\theta)}{2} + \epsilon_{c2,ASR}^o \frac{(1 - \cos 2\theta)}{2} \quad (3)$$

$$\epsilon_{cy,ASR}^o = \epsilon_{c1,ASR}^o \frac{(1 - \cos 2\theta)}{2} + \epsilon_{c2,ASR}^o \frac{(1 + \cos 2\theta)}{2} \quad (4)$$

$$\gamma_{cxy,ASR}^o = \epsilon_{c1,ASR}^o \sin 2\theta - \epsilon_{c2,ASR}^o \sin 2\theta \quad (5)$$

$$\epsilon_{cz,ASR}^o = \epsilon_{c3,ASR}^o \quad (6)$$

Thus, the prestrain vector for ASR is

$$[\epsilon_{c,ASR}^o] = \begin{bmatrix} \epsilon_{cx,ASR}^o \\ \epsilon_{cy,ASR}^o \\ \gamma_{cxy,ASR}^o \end{bmatrix} \quad (7)$$

The total prestrain vector $[\epsilon_c^o]$ is constructed through the summation of the thermal, shrinkage, post-cracking dilatation, and ASR-induced strains. Similar modifications can be performed for the three-dimensional case. The solution is then carried forward in the manner previously developed for the Disturbed Stress Field Model.²¹

Degradation of mechanical properties

Experimental data available in the literature show a reduction in strength and stiffness for ASR-affected concrete as compared to nonreactive concrete. Two options are available

to handle the changes in mechanical properties, reported to be influenced by the type of reactive aggregates, the environmental conditions, and the stress state. One alternative consists of directly using the value of the tested material properties in the analysis. The other option evaluates the compressive and tensile strengths, and the modulus of elasticity, as a function of the free expansion based on the ISE¹¹ prescriptions. With the latter, lower bounds to the mechanical properties have been defined using values from tests performed on cubes, prisms, and cylinders, and on cores extracted from structures. Both options disregard the directional nature of the degradation in mechanical properties caused by the stress level. Both approaches were implemented in the analysis programs.

VERIFICATION STUDIES

To verify that the ASR constitutive models and the analytical procedure were correctly implemented, and to explore their accuracy, analyses were conducted on representative ASR-affected specimens reported in the literature. The verification studies were performed at both the material and structural levels. The material-level investigation consisted of modeling the behavior of cylinders tested under uniaxial compression, and middle-notched prisms subjected to the three-point bending flexural loading, tested by Giaccio et al.²⁸ As part of the structural-level investigation, analyses were performed on flexural-critical reinforced concrete beams tested by Fan and Hanson,²⁹ and on shear-critical beams tested by Deschenes et al.⁴

Material-level investigation

Giaccio et al.²⁸ studied the mechanical behavior of concrete affected by ASR in comparison with the response of nonreactive concrete. Three different types of reactive concretes were designed with the same mixture proportions but with different reactive aggregates. Cylinders and prisms were cast and stored in saturated conditions at 38°C (100°F) to encourage ASR development. Longitudinal expansion measurements were performed on 75 x 75 x 300 mm (2.95 x 2.95 x 11.81 in.) prisms. Uniaxial compression tests were performed on 150 x 300 mm (5.91 x 11.81 in.) cylinders. Additional 100 x 200 mm (3.94 x 7.87 in.) cylinders were used to determine the compressive strength and modulus of elasticity at 28 days and their evolution with time. The stress-strain behavior in tension was studied through three-point bending tests of middle-notched prisms. The tests were performed at different ages of the specimens, for different levels of expansion. A major conclusion of this study was that specimens exhibiting the same level of expansion may reach substantially different compressive strength and stiffness, as shown in Table 1 for 150 x 300 mm (5.91 x 11.81 in.) cylinders.

The ASR developed in plain concrete under stress-free conditions and, thus, the expansion was uniform and the expansion model selected for the analyses had no influence on the results. As such, for both the compression and tension analyses, no distinction was made regarding the ASR model used.

One rectangular element was used to model the uniaxial compression tests. Nodal displacement-controlled loads with an increment of 0.01 mm (0.00039 in.) were applied

Table 1—Concrete properties²⁸

Specimen	Age, days	f'_c , MPa	E_c , MPa	Expansion ($\times 10^{-3}$)
C1	250	46.2	39,700	—
R2	200	37.3	19,900	1.45
R3	120	29.7	18,400	1.45
R4	745	49.7	28,800	1.35

Note: 1 MPa = 0.145 ksi.

Table 2—Default material properties

Concrete properties			
Thickness, mm	Required input	C_c ($^{\circ}C$)	10×10^{-6}
f'_c , MPa	Required input	Maximum aggregate size, mm	20
f'_t , MPa	$0.33\sqrt{f'_c}$	Density, kg/m ³	2400
E_c , MPa	$3320\sqrt{f'_c} + 6900$	G_f , kN/m	Bazant (2002) model
ϵ_o , mm/m	$1.8 + 0.0075 \cdot f'_c$	S_x , mm	1000
ν_o	0.15	S_y , mm	1000

Notes: Program limits to 1000 mm spacing of cracks parallel to y-axis, S_x and parallel to x-axis, S_y . Crack spacing is calculated based on CEB-FIP 1978 model; 1 kg/m³ = 1.686 lb/yd³; 1 kN/m = 68.522 lbf/ft.

at the two top nodes. The cylinder compressive strength and the modulus of elasticity were used as the concrete input parameters; the other properties were left as default values of the finite element program. For the reactive cylinders, the initial value of the displacement-controlled loads had to be adjusted according to the level of expansion of each mixture.

Shown in Fig. 2 are comparisons between the stress-strain relationships of four concrete specimens experimentally tested by Giaccio et al.²⁸ and those obtained numerically using three alternative concrete compression stress-strain response models—namely, Hognestad parabola, Attard and Setunge model,³⁰ and Popovics HSC model.³¹ As shown, the responses of Specimens C1, R2, and R3 computed with either the Hognestad or Attard and Setunge³⁰ models traced the observed response relatively well. The Popovics HSC model³¹ for high-strength concrete proved to be more appropriate for the R4 specimen, as it had a somewhat higher strength at 49.7 MPa (7.2 ksi).

Nine middle-notched prisms, 75 x 105 x 430 mm (2.95 x 4.13 x 16.93 in.), were used to determine the stress-strain behavior in tension. The prisms were modeled with a 5 x 5 mm (0.2 x 0.2 in.) mesh. A total of 1817 rectangular elements were used to represent the prisms, all having the same thickness of 105 mm (4.13 in.). Displacement-controlled load with 0.01 mm (0.00039 in.) increments was applied at the midspan. The material input parameters specified were the concrete compressive strength and modulus of elasticity, as determined from the cylinder tests performed on 100 x 200 mm (3.94 x 7.87 in.) cylinders. The other concrete properties were kept as program default values (Table 2). For the reactive specimens, the expansion determined on the 75 x 75 x 300 mm (2.95 x 2.95 x 11.81 in.) prisms was used to determine the strains caused by ASR. Shown in Table 3 are the material properties and expansion values for each prism specimen. Comparisons between the

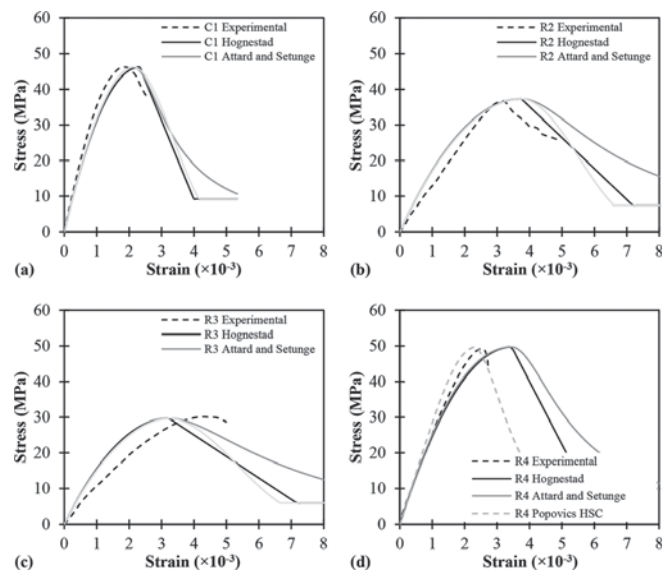


Fig. 2—Stress-strain behavior in compression: (a) nonreactive mixture C1; (b) reactive mixture R2; (c) reactive mixture R3; and (d) reactive mixture R4. (Note: 1 kN = 0.2248 kip; 1 mm = 0.0394 in.)

analytical results and the experimentally observed behaviors are shown in Fig. 3 for four specimens. Good correlation between the theoretical calculated behavior and the actual determined behavior can be observed; similar results were obtained for the remainder of the specimens.

The material-level finite element simulations show the behavior of reactive concrete subjected to pure compression or tension may be simulated to about the same level of accuracy as can be obtained for nonreactive concrete.

The accuracy of the ISE recommendations to predict the degradation of mechanical properties was evaluated against the specimens tested by Giaccio et al.²⁸ Table 3 presents the comparison between actual compressive strength and modulus of elasticity of the reactive concrete, and the ones estimated using the ISE reduction factors, as function of the free expansion and the concrete properties of nonreactive concrete at 28 days. It may be observed that ISE procedure underestimates the compressive strength, with the ratio of actual to calculated strengths having a mean of 1.79, and a coefficient of variation (COV) of 22%. The modulus of elasticity is estimated somewhat more accurately with a mean of 0.99 and a COV of 28%.

Reinforced concrete beams

Three beams, cast with reactive concrete, and three others with nonreactive concrete, were tested by Fan and Hanson.²⁹ Details of the specimens' properties are presented in Table 4. Two of the beams (#5N1 and #5N2) were loaded during the conditioning period such that cracks of approximately 0.2 mm (0.0079 in.) width developed on the tension face. After 1 year of accelerated conditioning, the beams were tested to failure.

A mesh sensitivity analysis was performed for Beam #3N, considered to be representative for all specimens. Shown in Fig. 4 is the comparison between the load-deflection behavior calculated with two different mesh densities. The analysis performed with a mesh size of 15 mm (having a

Table 3—Experimental²⁸ versus ISE estimated concrete properties

Specimen	Age, days	Expansion ($\times 10^{-3}$)	Experimental		ISE		Exp./ISE	
			f'_c , MPa	E_c , MPa	f'_c , MPa	E_c , MPa	f'_c	E_c
C1-28d	75	0.04	28.6	35,700	—	—	—	—
C1-250d	250	0.07	47.4	37,900	—	—	—	—
C1-745d	745	0.54	49.4	37,400	—	—	—	—
R2-200d	200	1.45	37.8	17,100	21.2	22,848	1.78	0.75
R2-250d	250	1.80	29.1	13,100	19.8	21,182	1.47	0.62
R3-75d	75	1.15	30.8	25,100	22.3	24,276	1.37	1.03
R3-120d	120	1.45	32.8	21,700	21.2	22,848	1.55	0.95
R4-485d	485	1.25	51.2	31,300	21.9	23,800	2.34	1.32
R4-745d	745	1.35	48.2	30,100	21.5	23,324	2.24	1.29
Mean							1.79	0.99
COV*, %							22	28

*COV is coefficient of variation.

Note: 1 MPa = 0.145 ksi.

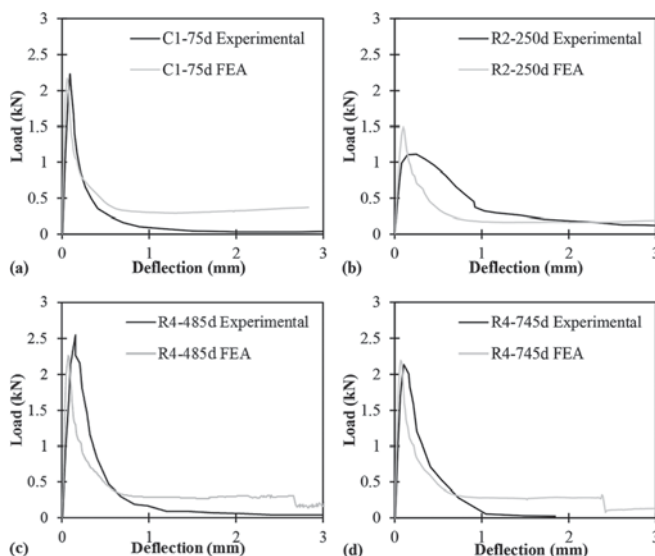


Fig. 3—Load-deflection behavior of prism specimens: (a) nonreactive mixture at 75 days; (b) reactive mixture R2 at 250 days; (c) reactive mixture R4 at 485 days; and (d) reactive mixture R4 at 745 days. (Note: 1 kN = 0.2248 kip; 1 mm = 0.0394 in.)

total of 1852 rectangular elements and 200 truss bars) and the analysis performed with a mesh size of 10 mm (with a total of 3766 rectangular elements and 292 truss bars) showed a maximum difference of 2.5% in calculated load and an insignificant difference in displacement. The results were considered acceptable, and the denser mesh was chosen for the rest of the analyses.

The longitudinal reinforcement was represented as discrete reinforcement, while the transverse reinforcement (that is, stirrups) was modeled as smeared. A bearing material with unidirectional stiffness was modeled at the interface between the bearing steel plates. Monotonically increasing nodal loads with 1.0 mm (0.039 in.) increments were applied to investigate the behavior of the beams. For the reactive spec-

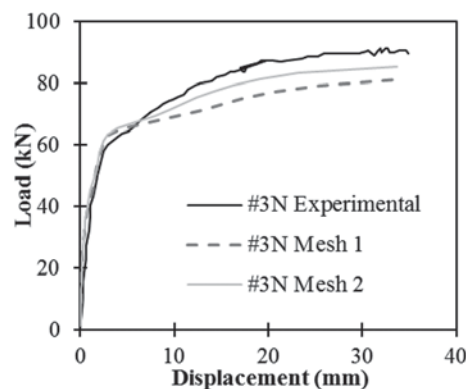


Fig. 4—Mesh sensitivity analysis for beam specimen #3N: Mesh 1 performed with 1852 elements; and Mesh 2 performed with 3766 elements. (Note: 1 kN = 0.2248 kip; 1 mm = 0.0394 in.)

imen conditioned under service load, loading was applied during the first load stage of the analysis, corresponding to the ASR expansion development. An increasing monotonic loading was then applied, representative of the test conditions. The results presented herein were obtained using the Saouma and Perotti model²⁶ for the ASR strain calculation. Similar results were obtained with all other implemented expansion models, except the model that evaluates the expansion uniformly in all directions, which yielded higher ASR strains.

Figure 5 presents the computed load-deformation response of the beam specimens compared to the experimentally measured behavior. As shown also in Table 4, the ultimate loads were estimated reasonably well with a mean of 1.08 and a COV of 3.1%. The computed responses overestimate the initial stiffness of the reactive beams, which may be a consequence of several factors: the prestressing effect of ASR on the reinforcement, the compressive stresses induced in concrete due to ASR expansion, and/or the overestimation of the modulus of elasticity for ASR-affected concrete. Although the analysis procedure inherently considers these

Table 4—Properties and results: Fan and Hanson²⁹ specimens

Specimen	Dimensions*			Material properties [†]			Results		
	<i>b</i> , mm	<i>h</i> , mm	Span, mm	ρ_{long} , %	ρ_{vert} , %	f'_c , MPa	$P_{u,exp}$, kN	$P_{u,calc}$, kN	Exp./Calc.
#3N	150	250	1473	0.4	0.34	34.7	89.6	85.4	1.05
#3R				0.4		27.2	86.5	79.4	1.09
#5N1				1.0		34.7	184.3	177.4	1.04
#5R1				1.0		27.2	178	161.4	1.10
#5N2				1.0		34.7	190	177.4	1.07
#5R2				1.0		27.2	188.2	165.4	1.14
								Mean	1.08
								COV [‡] , %	3.08

**b* is cross-sectional width; *h* is cross-sectional height.

[†] ρ_{long} is longitudinal reinforcement ratio; ρ_{vert} is vertical reinforcement ratio.

[‡]COV is coefficient of variation.

Notes: 1 mm = 0.0394 in.; 1 MPa = 0.145 ksi; 1 kN = 0.2248 kip.

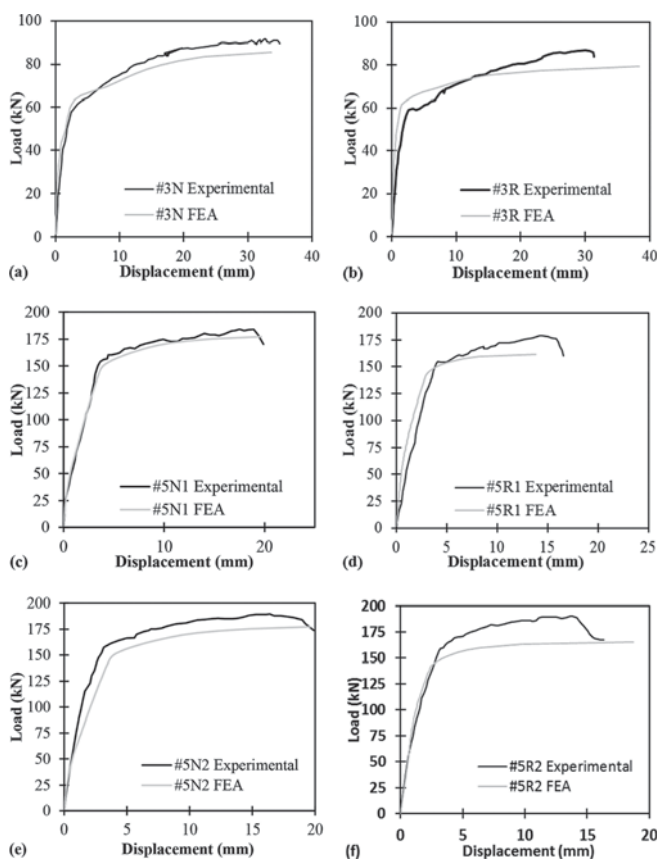


Fig. 5—Load-deformation responses of Fan and Hanson²⁹ beam specimens. (Note: 1 kN = 0.2248 kip; 1 mm = 0.0394 in.)

factors, the currently available constitutive models may not adequately represent them.

Further corroboration was done through the tests conducted by Deschenes et al.⁴ Six specimens, and a pilot specimen, were constructed: four of them were cast with reactive concrete and cured at high temperatures while the remaining two nonreactive specimens were used as a basis for comparison of long-term structural performance. Two independent shear tests—a deep beam shear test and a sectional shear test—were performed on each specimen, one at each end. Details of the specimens are summarized in Table 5.

The typical finite element mesh is shown in Fig. 6, with a total of 3842 rectangular elements and 672 truss bar elements. The mesh size was chosen according to previous studies on shear-critical beams,³² by dividing the beam into at least 15 elements through the depth and maintaining a maximum aspect ratio of 2.0. Increasing the number of elements to 5646 did not have a significant effect on the results, for neither the sectional shear tests nor the deep beam tests, with a maximum difference of 2.2% for the calculated capacity.

Two analyses were performed for each shear test, the variables being the concrete properties. In the first case, the compressive strength, as determined from cylinders at the time of the beams tests, together with the initial tangent modulus of elasticity, were the input values. For the second analysis, the targeted compressive strength at 28 days was used together with the initial tangent modulus of elasticity; to account for the changes in mechanical properties due to ASR, the reduction functions suggested by ISE were used. Four of the specimens were tested with respect to damage severity: undamaged, mild, and moderate. The development of ASR/DEF was dominated by the in-plane expansion in the transverse direction, similar to the behavior reported in other studies.³³ Two factors were considered to contribute to this anisotropy: the amount of reinforcement in the longitudinal direction, significantly larger than the amount of reinforcement in transverse direction, and the vertical casting direction. The comparison between the calculated ASR-induced strains and the measured strains is shown in Table 6, as obtained using Saouma and Perotti model.²⁶ No significant difference in results was observed as a result of the choice of expansion model, except for the model that assumes uniform strain distribution, which yielded higher expansion. This was consistent with the results obtained for the Fan and Hanson²⁹ specimens.

The ultimate loads obtained from the theoretical analysis are compared with the experimental values in Table 5. The free expansions at the time of testing, determined from corresponding cylinders, were input for both reactive beams. It may be observed that the use of the ISE ASR-correlated reduction factors for the compressive strength, tensile

Table 5—Properties and results: Deschenes et al.⁴ specimens

Deep beam shear spans											
	Dimensions*			Material properties [†]			$P_{u,exp.}$, kN	$P_{u,calc.}$, kN		Exp./Calc.	
	b , mm	h , mm	Span, mm	$\rho_{long.}$, %	$\rho_{vert.}$, %	f'_c , MPa		Actual [‡]	Factored [§]	Actual [‡]	Factored [§]
Pilot	533	1067	1697	3.1	0.31	35.2	2630	1981		1.32	
nR1						50.3	2500	2235		1.12	
R1						31.7	2309	2754	2176	0.84	1.06
R2						26.9	2440	2910	2363	0.84	1.03
									Mean	1.03	1.13
									COV , %	22.7	11.5

Sectional shear spans											
	Dimensions			Material properties			$P_{u,exp.}$, kN	$P_{u,calc.}$, kN		Exp./Calc.	
	b , mm	h , mm	Span, mm	$\rho_{long.}$, %	$\rho_{vert.}$, %	f'_c , MPa		Actual [‡]	Factored [§]	Actual [‡]	Factored [§]
Pilot	533	1067	2753	3.1	0.15	35.8	1303	1359		0.96	
nR1						49.6	1230	1504		0.82	
R1						31.0	1496	1767	1486	0.85	1.00
R2						28.9	1570	1890	1576	0.83	0.99
									Mean	0.87	0.93
									COV , %	7.5	8.9

* b is cross-sectional width; h is cross-sectional height.

[†] $\rho_{long.}$ is longitudinal reinforcement ratio; $\rho_{vert.}$ is vertical reinforcement ratio.

[‡]Actual: concrete properties obtained from cylinder tests.

[§]Factored: concrete properties calculated using ISE reduction functions.

^{||}COV is coefficient of variation.

Notes: 1 mm = 0.0394 in.; 1 MPa = 0.145 ksi; 1 kN = 0.2248 kip.

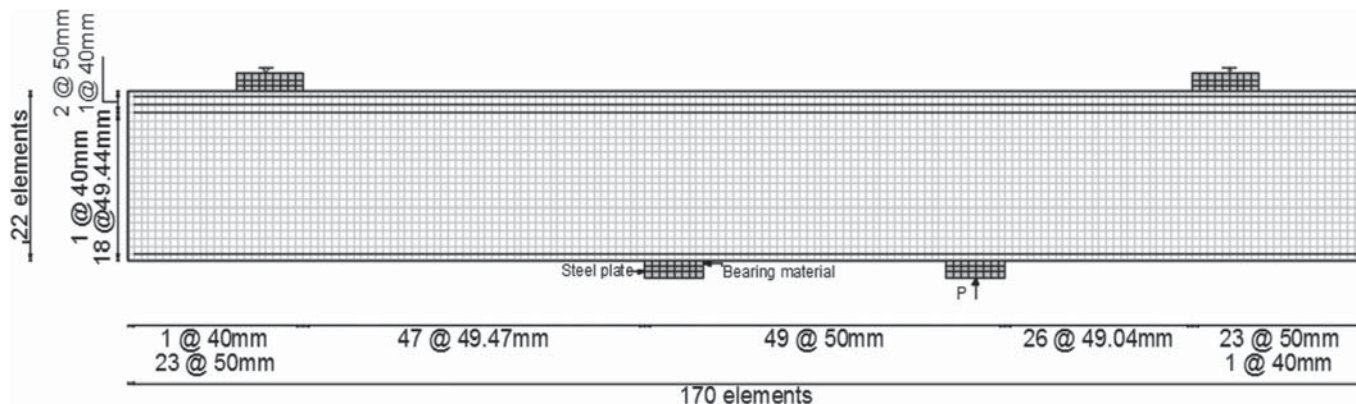


Fig. 6—Finite element model for Deschenes et al.⁴ reinforced concrete beam specimens. (Note: 1 mm = 0.0394 in.)

strength, and modulus of elasticity led to better correlations to the experimental values than was obtained by using material properties determined from tests on cores or cylinders.

An experimental program is currently ongoing at the University of Toronto, investigating the behavior of reactive shear walls. Further verification studies will be performed in the future by simulating their response.

ASPECTS IN NEED OF FURTHER RESEARCH

The primary purpose of this paper was to develop and verify a numerical procedure for modeling and assessment of ASR-affected structures. In doing so, some limitations and deficiencies were found; these stemmed not so much

from deficiencies in the analytical approach, but rather in the constitutive models for ASR-affected concrete currently available in the literature. Accordingly, the following recommendations are made for further improving our computational capabilities:

1. Reductions in the concrete mechanical properties are likely non-uniform in the principal directions due to the anisotropic expansion.^{7,11,34} This aspect was not accounted for in the work presented herein, nor is it in other analyses reported in the literature. Relationships that capture the ASR-induced anisotropy of the material are required.
2. It is known that the aggregate type has an influence on the mechanical properties. This influence has not been

Table 6—ASR/DEF expansion: experimental⁴ versus calculated strains

Specimen	Experimental				Calculated			
	ϵ_{ct}^* ($\times 10^{-3}$)	ϵ_{cl}^\dagger ($\times 10^{-3}$)	ϵ_{st}^\ddagger ($\times 10^{-3}$)	ϵ_{sl}^\S ($\times 10^{-3}$)	ϵ_{ct}^* ($\times 10^{-3}$)	ϵ_{cl}^\dagger ($\times 10^{-3}$)	ϵ_{st}^\ddagger ($\times 10^{-3}$)	ϵ_{sl}^\S ($\times 10^{-3}$)
R1 DB	1.70	0.60	1.00	0.40	1.40	0.45	1.02	0.45
R2 DB	4.50	0.70	4.50	0.90	4.50	0.65	4.50	0.90
R1 SS	1.90	0.70	1.80	0.50	1.70	0.60	1.75	0.45
R2 SS	6.90	0.20	6.80	0.70	5.00	0.70	6.90	0.80

* ϵ_{ct} is transverse concrete strain.

† ϵ_{cl} is longitudinal concrete strain.

‡ ϵ_{st} is transverse steel strain.

§ ϵ_{sl} is longitudinal steel strain.

properly captured by experimental studies, nor is it currently considered in analytical procedures.

3. Bond degradation is expected to occur as a result of ASR, but this issue is not currently addressed in the literature. The development and implementation of appropriate bond models for ASR-affected concrete would be of value for structural elements that are susceptible to bond slip.

4. The influence of tensile stresses on the induced expansion is currently considered in only one of the models implemented: the Curtis model. However, it was formulated based on cursory field observations and is only suitable for linear elastic analysis procedures where post-cracking behavior is not explicitly considered. Further investigation into the influences of tensile stresses and cracking are required.

5. The influence of ASR on Poisson's effect is not currently quantified. An appropriate model that captures this influence is required, as it would have a significant effect on the levels of confinement calculated.

6. The increase in strength of some shear-critical specimens may be attributed to the confinement effect caused by either the transverse reinforcement in the case of beams or the boundary elements in the case of shear walls. However, the ductility in shear-critical concrete structures affected by ASR is also a potential concern. Thus, it would be of interest to study the response of ASR-affected concrete subjected to shear stresses that were allowed free expansion during the ASR development phase.

CONCLUSIONS

Based on the results of the analyses performed, several conclusions and observations can be made:

1. A smeared rotating-crack conceptual model for concrete, incorporated into a total-load secant-stiffness macro-modeling framework, is a viable NLFEA strategy for modeling ASR effects on reinforced concrete structures.

2. The Disturbed Stress Field Model provides a workable platform on which ASR constitutive models can be implemented.

3. The magnitude and direction of the induced strains depend on internal and external restraints as well as on long-term loading conditions, and must be appropriately considered for the ASR analysis.

4. Strength and stiffness degradation can be taken into account by either employing reduction factors, as recommended by ISE, or by using the measured properties from samples or cores. Current evidence suggests that neither

approach performs consistently better than the other when analyzing ASR-affected specimens.

5. The material-level investigation revealed that the ISE reduction factors tend to underestimate the value of the compressive strength for ASR-affected specimens, while the modulus of elasticity is predicted more accurately.

6. Confinement conditions have a significant influence on the results. Special care should be taken in modeling confinement related mechanisms, such as Poisson's effect and strength and stiffness enhancement, in a realistic fashion.

7. The flexural-critical specimens²⁹ analyzed did not exhibit a significant reduction in either capacity or ductility due to ASR.

8. Some shear-critical specimens, such as shear walls and reinforced concrete beams provided with transverse reinforcement, showed an increase in strength caused by ASR; an opposite effect was observed in beams with no stirrups.

9. The strains developed due to ASR were predicted relatively well. The mean experimental-to-calculated ratio of the ASR-induced strains for the analyzed specimens was 1.03 with a COV of 16.3%.

10. At the material level, with the exception of the model that evaluates ASR-induced expansion uniformly in all directions, the models yielded similar results. Additionally, no significant difference in accuracy of results was observed between the expansion models at the structural level.

11. Currently, the developed procedure shows reasonable accuracy in modeling the response of ASR-affected structures. For the flexural-critical specimens²⁹ analyzed, it gave strengths with a mean experimental-to-calculated ratio of 1.08 and a COV of 3.1%. The mean experimental-to-calculated ratio for the ultimate loads of the shear-critical beams⁴ analyzed was 0.99 and a COV of 12.6%.

12. To achieve improved accuracy and reliability in the analysis capabilities, additional work is required in better describing the constitutive response of ASR-affected concrete.

AUTHOR BIOS

Anca C. Ferche is a PhD Student in the Department of Civil Engineering at the University of Toronto, Toronto, ON, Canada. She received her BASC from the Technical University of Cluj-Napoca, Cluj-Napoca, Romania; and her MASC from the University of Toronto. Her research interests include performance assessment and analysis of reinforced concrete structures, concrete deterioration mechanisms, and rehabilitation of structures.

ACI member **Daman K. Panesar** is an Associate Professor in the Department of Civil Engineering at the University of Toronto. Her research inter-

ests include advancing concrete materials, low-carbon materials, material characterization, and durability performance of aging infrastructure.

Shamim A. Sheikh, *FACI*, is a Professor of civil engineering at the University of Toronto. He is a past Chair and member of Joint ACI-ASCE Committee 441, Reinforced Concrete Columns, and a member of ACI Committee 374, Forwork for Concrete. He received the ACI Chester Paul Seiss Award for Excellence in Structural Research in 1999. His research interests include earthquake resistance and design of concrete structures, concrete confinement, and use of fiber-reinforced polymer for sustainable concrete structures.

Frank J. Vecchio, *FACI*, is a Professor in the Department of Civil Engineering at the University of Toronto. He is a member of Joint ACI-ASCE Committees 441, Reinforced Concrete Columns, and 447, Finite Element Analysis of Reinforced Concrete Structures. He received the following ACI awards: Chester Paul Seiss Award for Excellence in Structural Research in 1998; ACI Design Award in 1999; Wason Medal for Most Meritorious Paper in 2011; and the Joe W. Kelley Award in 2016. His research interests include advanced constitutive modeling and analysis of reinforced concrete, assessment and rehabilitation of structures, and response to extreme loads.

ACKNOWLEDGMENTS

The authors wish to express their gratitude to the Canadian Nuclear Safety Commission (CNSC), which funded this research. This paper represents the opinions of the authors and it is not the technical position of the CNSC.

REFERENCES

1. Stanton, T. E., "Expansion of Concrete Through Reaction between Cement and Aggregate," *Proceedings of the American Society of Civil Engineers*, pp. 1781-1811. Reprinted with discussion and closure in *Transaction*, ASCE, V. 107, 1940, pp. 54-126.
2. Stanton, T. E., "California Experience with the Expansion of Concrete through Reaction between Cement and Aggregate," *ACI Journal Proceedings*, V. 38, No. 3, Jan. 1942, pp. 209-215.
3. Swenson, E. G., "A Reactive Aggregate Undetected by ASTM Tests," *ASTM Bulletin*, V. 226, 1957, pp. 48-57.
4. Deschenes, D. J.; Bayrak, O.; and Folliard, K. J., "ASR/DEF – Damaged Bent Caps: Shear Tests and Field Implications," *Technical Report No. 12-8XXIA006*, 2009, 271 pp.
5. Shayan, A., and Ivanusec, I., "An Experimental Clarification of the Association of Delayed Ettringite Formation with Alkali-Aggregate Reaction," *Cement and Concrete Composites*, V. 18, No. 3, 1996, pp. 161-170. doi: 10.1016/0958-9465(96)00012-1
6. Bouzabata, H.; Multon, S.; Sellier, A.; and Houari, H., "Swellings due to Alkali-Silica Reaction and Delayed Ettringite Formation: Characterisation of Expansion Isotropy and Effect of Moisture Conditions," *Cement and Concrete Composites*, V. 34, No. 3, 2012, pp. 349-356. doi: 10.1016/j.cemconcomp.2011.10.006
7. Gautam, B., "Multiaxially Loaded Concrete Undergoing Alkali Silica Reaction (ASR)," PhD thesis, University of Toronto, Toronto, ON, Canada, 2016, 196 pp.
8. Sanchez, L.; Fournier, B.; Jolin, M.; Bedoya, M. A. B.; Bastien, J.; and Duchesne, J., "Use of Damage Rating Index to Quantify Alkali-Silica Reaction Damage in Concrete: Fine versus Coarse Aggregate," *ACI Materials Journal*, V. 113, No. 4, July-Aug. 2016, pp. 395-407. doi: 10.14359/51688983
9. Rivard, P., and Ballivy, G., "Assessment of the Expansion Related to Alkali-Silica Reaction by the Damage Rating Index Method," *Construction and Building Materials*, V. 19, No. 2, 2005, pp. 83-90. doi: 10.1016/j.conbuildmat.2004.06.001
10. Rivard, P., and Saint-Pierre, F., "Assessing Alkali-Silica Reaction Damage to Concrete with Non-destructive Methods: From the Lab to the Field," *Construction and Building Materials*, V. 23, No. 2, 2009, pp. 902-909. doi: 10.1016/j.conbuildmat.2008.04.013
11. Institution of Structural Engineers (ISE), "Structural Effects of Alkali-Silica Reaction," SETO, London, UK, 1992, 36 pp.
12. Bažant, Z. P., and Steffens, A., "Mathematical Model for Kinetics of Alkali-Silica Reaction in Concrete," *Cement and Concrete Research*, V. 30, No. 3, 2000, pp. 419-428. doi: 10.1016/S0008-8846(99)00270-7
13. Çopuroğlu, O., and Schlangen, E., "Modelling of Effect of ASR on Concrete Microstructure," *Key Engineering Materials*, V. 348, 2007, pp. 809-812. doi: 10.4028/www.scientific.net/KEM.348-349.809
14. Puatatsananon, W., and Saouma, V., "Chemo-Mechanical Micro-model for Alkali-Silica Reaction," *ACI Materials Journal*, V. 110, No. 1, Jan.-Feb. 2013, pp. 67-77.
15. Dunant, C. F., and Scrivener, K. L., "Micro-Mechanical Modelling of Alkali-Silica-Reaction-Induced Degradation Using the AMIE Framework," *Cement and Concrete Research*, V. 40, No. 4, 2010, pp. 517-525. doi: 10.1016/j.cemconres.2009.07.024
16. Ulm, F.; Coussy, O.; Kefei, L.; and Larive, C., "Thermo-Chemo-Mechanics of ASR Expansion in Concrete Structures," *Journal of Engineering Mechanics*, ASCE, V. 126, No. 3, 2000, pp. 233-242. doi: 10.1061/(ASCE)0733-9399(2000)126:3(233)
17. Grimal, E.; Sellier, A.; Le Pape, Y.; and Bourdarot, E., "Creep, Shrinkage, and Anisotropic Damage in Alkali-Aggregate Reaction Swelling Mechanism—Part I: A Constitutive Model," *ACI Materials Journal*, V. 105, No. 3, May-June 2008, pp. 227-235.
18. Farage, M. C. R.; Alves, J. L. D.; and Fairbairn, E. M. R., "Macroscopic Modelling of Concrete Subjected to Alkali-Aggregate Reaction," *Cement and Concrete Research*, V. 34, No. 3, 2004, pp. 495-505. doi: 10.1016/j.cemconres.2003.09.001
19. Fairbairn, E. M. R.; Ribeiro, F. L. B.; Lopes, L. E.; Toledo-Filho, R. D.; and Silvano, M. M., "Modelling the Structural Behaviour of a Dam Affected by Alkali-Silica Reaction," *Communications in Numerical Methods in Engineering*, V. 22, No. 1, 2006, pp. 1-12. doi: 10.1002/cnm.788
20. Vecchio, F. J., and Collins, M. P., "The Modified Compression Field Theory for Reinforced Concrete Elements Subjected to Shear," *ACI Journal Proceedings*, V. 83, No. 2, Mar.-Apr. 1986, pp. 219-231.
21. Vecchio, F. J., "Disturbed Stress Field Model for Reinforced Concrete: Formulation," *Journal of Structural Engineering*, ASCE, V. 126, No. 9, 2000, pp. 1070-1077. doi: 10.1061/(ASCE)0733-9445(2000)126:9(1070)
22. Vecchio, F. J., "Nonlinear Finite Element Analysis of Reinforced Concrete Membranes," *ACI Structural Journal*, V. 86, No. 1, Jan.-Feb. 1989, pp. 26-35.
23. Vecchio, F. J., "Reinforced Concrete Membrane Element Formulations," *Journal of Structural Engineering*, ASCE, V. 116, No. 3, 1990, pp. 730-750. doi: 10.1061/(ASCE)0733-9445(1990)116:3(730)
24. Vecchio, F. J., "Finite Element Modeling of Concrete Expansion and Confinement," *Journal of Structural Engineering*, ASCE, V. 118, No. 9, 1992, pp. 46-56. doi: 10.1061/(ASCE)0733-9445(1992)118:9(2390)
25. Charwood, R. G.; Solymar, S. V.; and Curtis, D. D., "A Review of Alkali Aggregate Reactions in Hydroelectric Plants and Dams," *Proceedings of the International Conference of Alkali-Aggregate Reactions in Hydroelectric Plants and Dams*, Fredericton, NB, Canada, 1992, pp. 129-135.
26. Saouma, V., and Perotti, L., "Constitutive Model for Alkali-Aggregate Reactions," *ACI Materials Journal*, V. 103, No. 3, May-June 2006, pp. 194-202.
27. Sellier, A.; Bourdarot, E.; Multon, S.; Cyr, M.; and Grimal, E., "Combination of Structural Monitoring and Laboratory Tests for Assessment of Alkali-Aggregate Reaction Swelling: Application to Gate Structure Dam," *ACI Materials Journal*, V. 106, No. 3, May-June 2009, pp. 281-290.
28. Giaccio, G.; Zerbino, R.; Ponce, J. M.; and Batic, O. R., "Mechanical Behavior of Concretes Damaged by Alkali-Silica Reaction," *Cement and Concrete Research*, V. 38, No. 7, 2008, pp. 993-1004. doi: 10.1016/j.cemconres.2008.02.009
29. Fan, S., and Hanson, J. M., "Effect of Alkali Silica Reaction Expansion and Cracking on Structural Behavior of Reinforced Concrete Beams," *ACI Structural Journal*, V. 95, No. 5, Sept.-Oct. 1998, pp. 498-505.
30. Attard, M., and Setunge, S., "Stress-Strain Relationship of Confined and Unconfined Concrete," *ACI Materials Journal*, V. 93, No. 6, Nov.-Dec. 1996, pp. 432-442.
31. Thorenfeldt, E.; Tomaszewicz, A.; and Jensen, J. J., "Mechanical Properties of High-Strength Concrete and Application in Design," *Proceedings of the Symposium Utilization of High Strength Concrete*, Stavanger, Norway, June 1987, pp. 149-159.
32. Saatci, S., and Vecchio, F. J., "Nonlinear Finite Element Modeling of Reinforced Concrete Structures under Impact Loads," *ACI Structural Journal*, V. 106, No. 5, Sept.-Oct. 2009, pp. 717-725.
33. Multon, S.; Seignol, J. F.; and Toutlemonde, F., "Structural Behavior of Concrete Beams Affected by Alkali-Silica Reaction," *ACI Materials Journal*, V. 102, No. 2, Mar.-Apr. 2005, pp. 67-76.
34. CSA Special Publication A844-00, "Guide to the Evaluation and Management of Concrete Structures Affected by Alkali-Aggregate Reaction," Canadian Standards Association, Toronto, ON, Canada, 2000, 121 pp.